Episodic slowdown of global warming by a multi-year La Niña

Tomoki Iwakiri[a,b] and Tsubasa Kohyama[b,c]

[a] *International Pacific Research Center, University of Hawai'i at Mānoa, Honolulu.*

[b] *Faculty of Core Research Natural Sciences Division, Ochanomizu University, Tokyo, Japan.*

[c] *Department of Information Sciences, Ochanomizu University, Tokyo, Japan.*

Corresponding author: Tomoki Iwakiri, iwakirit@hawaii.edu

May 12 2026, Accepted to *Journal of Climate*

ABSTRACT

Global mean surface temperature (GMST), which has continued to rise due to the anthropogenic greenhouse gas forcing, is closely related to the sea surface temperature variability in the tropical Pacific. In particular, GMST is known to increase during a strong and short-lived El Niño. By contrast, the global cooling effect of a weak and long-lived La Niña remains underexplored, particularly that of multi-year La Niña. This study shows that multi-year La Niña events tend to have a strong cooling effect on GMST based on observations and climate model simulations. The minimum of GMST around the second-year La Niña becomes larger despite the comparable or weaker amplitude of La Niña. The persistent La Niña cools the pantropical climate, causing a temporary GMST warming stagnancy, whereas the cooling effect of a single-year La Niña is weaker due to the lagged response of other tropical basins and its transience. Yet, even during so-called triple-dip or longer events, global cooling can persist despite the modest La Niña forcing, because the pan-tropical climate has already been cooled. Applying the resistor–capacitor (RC)-framework analogy, we demonstrate that the lagged decreases in GMST and its lower bound during multi-year La Niña episodes arise naturally from the climate system's intrinsic transient sensitivity and the heat capacity of the ocean mixed layer. The RC framework would offer a simple, intuitive, and pedagogically useful tool for interpreting the GMST response to ENSO.

1. Introduction

Global mean surface temperature (GMST) is the most widely used integrative metric of Earth and planetary science (IPCC 2021). It provides a common baseline for comparing climates across eras, regions, and even planets. As a spatial average over land and ocean surfaces, GMST condenses myriad processes, such as radiative forcing by greenhouse gases, aerosols, water-vapor and cloud feedbacks, ocean heat uptake, and cryosphere changes, into a single, policy-salient indicator. International temperature targets aimed at constraining climate change are framed in terms of GMST anomalies relative to a pre-industrial baseline, and detection-and-attribution assessments routinely rely on its evolution to quantify the human fingerprint on climate.

GMST has been rising for more than a century (Osman et al. 2021). The anthropogenic greenhouse gas imposes a radiative imbalance and warms the planet. However, the pace of global warming is not constant and occasionally slows down. While irregular anthropogenic

forcings and intermittent volcanic forcings can modulate GMST, natural climate variability also modulates the global warming rate. A decadal hiatus of global warming observed in the 2000s was caused by lower-than-average sea surface temperatures (SSTs) in the eastern Pacific (Kosaka and Xie 2013) and GMST change exhibits a staircase-like shape following the natural decadal variability (Kosaka and Xie 2016; Meehl et al. 2011; Watanabe et al. 2014), which is referred to as the Interdecadal Pacific Oscillation (IPO) (Power et al. 1999; Zhang et al. 1997).

Interannual SST variability in the tropical Pacific, as distinct from decadal fluctuations, is predominantly caused by the El Niño-Southern Oscillation (ENSO) (Walker 1923; Bjerknes 1966). Due to the existence of ENSO, SSTs in the equatorial eastern Pacific oscillate between warm and cool phases, which are referred to as the El Niño and La Niña events, respectively. ENSO controls tropospheric temperature over the tropics on the interannual time scale (Horel and Wallace 1981; Pan and Oort 1983; Yulaeva and Wallace 1994; Sobel 2002). When a strong El Niño occurs, GMST tends to be high since heat stored in the upper ocean is released into the atmosphere (Trenberth et al. 2002; Thompson et al. 2009). ENSO exhibits an asymmetry between El Niños and La Niñas (An and Jin 2004; Kohyama and Hartmann 2017; Timmermann et al. 2018); El Niño events tend to be strong and short-lived, whereas La Niña events tend to be weak and long-lived (Larkin and Harrison 2002). Compared to stochastic wind-driven strong El Niño events, strong La Niña events are more tightly linked to slowly varying thermocline variability, offering a clearer source of long-lead predictability and a compelling target (Dommenget et al. 2013).

In this study, we shed light on the longevity of a La Niña, rather than a short-lived El Niño, in determining GMST. In recent years, the ENSO research community has paid much attention to the so-called “multi-year La Niña”, during which the La Niña phase persists for more than a year (DiNezio and Deser 2014; Iwakiri and Watanabe 2021, 2022; Kim et al. 2023; Park et al. 2020; Wu 2020; Fasullo et al. 2023). Multi-year La Niña events are known to cause regionally distinct responses (Cole 2002; Okumura et al. 2017; Iwakiri and Watanabe 2020; Jiang et al. 2025). However, while the ENSO‑GMST relationship has been extensively studied, to the best of our knowledge, the impact of a multi-year La Niña on GMST has not been specifically examined. Multi-year La Niña events could have a relatively strong cooling effect on GMST, because they are expected to cool the atmosphere longer than single-year events. Recent studies emphasized a global warming spike-driven by strong El Niño events (Hu and Fedorov 2017; Raghuraman et al. 2024; Jiang et al. 2025; Tsuchida et al. 2026), but strong El Niño events are often followed by multi-year La Niña (Wu et al. 2019; Iwakiri and Watanabe 2021), so the

resulting GMST spike is expected to be transient. As observed multi-year La Niña events provide limited samples, we analyze multi-model large-ensemble (MMLE) simulations spanning eleven models with 20–100 ensemble members each, yielding more than 30,000 model years. This dataset isolates internal climate variability, by removing the common forced signals of human activities, volcanic eruption and so on, and ensures a sufficient number of events.

The manuscript is organized as follows. Section 2 describes the observational datasets and models used. Section 3 investigates the GMST response to La Niña persistence using these data and models. Section 4 evaluates this response with a conceptual framework, and Section 5 demonstrates the utility of that model by reproducing the historical response. Section 6 presents the discussion.

2. Data and methods

a. Observational and reanalysis data sets

We use the Goddard Institute for Space Studies surface temperature analysis version 4 (GISTEMPv4) (Lenssen et al. 2019) for surface air temperature (SAT), and the Extended Reconstruction SST version 6 (ERSSTv6) (Huang et al. 2025a,b) for SST. SAT is used to calculate GMST. Anomalies are defined as deviations from the monthly climatology, which is calculated for each month as a long-term mean over the period from 1950 through 2024, except for GISTEMPv4. GISTEMPv4 is provided as anomalous surface temperatures relative to the 1951-1980 climatology. Quadratic detrending is applied to remove the global warming effect. This study focuses primarily on the last 75 years (1950–2024) because the proportion of missing data varies significantly before 1950, which may cause uncertainties in estimating the GMST, particularly in terms of regional contributions (Fig. S1). Also, our conclusion is not sensitive to selected period demonstrated in the multi-model ensemble (see below).

b. Multi-model large ensemble simulations

We utilize a collection of single model initial-condition large ensemble simulations from the multi-model large ensemble archive version 2 (Maher et al. 2024), conducted with the Coupled

Model Intercomparison Project (CMIP). We use six CMIP5-class Global Climate Models (GCMs) (Taylor et al. 2012), CanESM2 (Kirchmeier-Young et al. 2017), CESM1-CAM5 (Kay et al. 2015), CSIRO-Mk3-6-0 (Jeffrey et al. 2013), GFDL-CM3 (Sun et al. 2018), GFDL-ESM2M (Rodgers et al. 2015), and MPI-ESM (Maher et al. 2019), and five CMIP6-class GCMs (Eyring et al. 2016), ACCESS-ESM1-5 (Ziehn et al. 2020), CanESM5 (Swart et al. 2019), MIROC6 (Tatebe et al. 2019), MPI-ESM1-2-LR (Olonscheck et al. 2023), GFDL-SPEAR-MED (Bethke et al. 2021). The models are forced by historical forcings, the Representative Concentration Pathway 8.5 (RCP8.5) for CMIP5 models, and the Shared Socioeconomic Pathway (SSP) 5-8.5 scenario for CMIP6 models. The period of simulations from 1950 to 2024 is used, and all models include a sufficient number of ensembles, more than 20, to extract the external forced signals (See Table S1). The forced component of the model simulations is defined as the ensemble mean and is subtracted from each simulated output to isolate pure internal variability. We analyze the period from 1950 to 2024, but it is not sensitive to the selected period (Fig. S2). The externally forced signal arising from differences among the future scenarios emerges mainly from the mid-21st century onward and therefore the choice of future scenario does not affect the results. Also, we use mixture of RCP8.5 and SSP5-8.5 scenarios, but even separate analysis leads to the same conclusion, indicating independence on emission scenario (Fig. S3).

c. Definition of ENSO

ENSO is measured based on the time series of SST anomalies averaged over the Niño 3.4 region (170°W-120°W, 5°S-5°N), called the Niño 3.4 index. La Niña events are extracted if the October-February (ONDJF)-mean Niño 3.4 index falls below −0.5 standard deviation as considering ENSO amplitude varies across observation and each model. A multi-year La Niña is defined as a La Niña event that continues for two or three consecutive years, called the double-dip and triple-dip La Niñas, respectively (Iwakiri and Watanabe 2022). Extracted observed La Niña is shown in Table S2. As triple-dip La Niña events are rare in observation, only three samples are extracted during 1950-2024 (1973-76, 1998-2001, 2020-23). Note, even when the observational analysis is extended to 1900–2024, only four triple-dip La Niña events are identified, so the statistics change little. To account for greater uncertainties in early–20th century observations and availability of MMLE datasets (Fig. S1), our baseline analysis focuses on 1950–2024. The first year of the composited La Niña is denoted as the Year 0. The

number of detected ENSO events also varies across models, but for MMLE-mean, we first take ensemble-mean, and then take multi-model mean to treat each model equally.

d. Significance test

The statistical significance and confidence interval are evaluated using bootstrap tests with 1,000 resampling iterations. For models with multiple ensemble members, the ensemble-mean of each metric is first calculated. Then, bootstrapping is applied across the multi-model ensemble, treating each model equally. Also, the statistical significance of composite analysis is assessed, and *p*-values are calculated for each individual model. A combined *p*-value for the MME-mean composite is derived from the Stouffer Z-score method (Stouffer et al. 1949).

3. GMST response to a multi-year La Niña

GMST has increased under anthropogenic forcing (Fig. 1), yet the rate of increase is modulated by internal climate variability. Multi-year La Niña episodes have recurred with notable frequency over the past 75 years and often persist for two to three years. During these episodes, GMST typically dips, thereby exerting a transient cooling influence that temporarily slows the apparent warming trend on event timescales. When the annual mean is defined from July to June to better follow the ENSO life cycle, a consistent decrease in GMST is found between the first and second La Niña dips (Fig. S4).

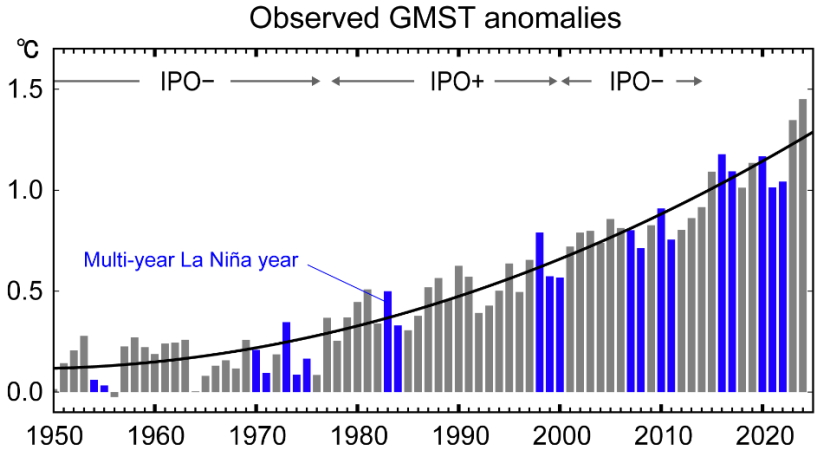

Figure 1. Historically observed annual-mean (calendar-year) global-mean surface temperature (GMST) anomalies relative to 1850-1900, obtained by adding a 0.19°C offset following the NASA GISS guide. Blue bars are multi-year La Niña years. Black line is the quadratic trend.

Figure 2 shows the GMST response to La Niña persistence. In observations, the GMST response to a single-year La Niña lags the event peak (November–December–January), reaching its minimum in boreal winter (December–January–February, DJF) with a drop of approximately −0.11°C. When La Niña persists for two consecutive years, so-called double-dip La Niña, the cooling lasts correspondingly longer and the minimum deepens to roughly −0.16°C. The amplitude of the second-year La Niña is comparable to that of the first year. Although only a few triple-dip La Niña events are observed, the GMST cooling persists even further, with large uncertainty.

Given the small number of observed cases, we extend the analysis to MMLE simulations. The large-ensemble framework removes the common forced signal of both anthropogenic forcing and volcanic eruption and isolates internal variability, providing many realizations and substantially narrowing uncertainty. Across models, single-year La Niña events decrease GMST by −0.11°C on average with small uncertainty. During double-dip La Niña, the cooling lasts longer and the minimum occurs during the second year, deepening to −0.18°C, which is statistically significantly larger in magnitude than for single-year events. These GMST amplitudes are quantitatively consistent with observations. It should be noted that the amplitude of the second-year La Niña is smaller than that of the first year. For the triple-dip cases, GMST decreases for three years, but the minimum occurs in the second year at −0.18°C and is comparable to that of the double-dip La Niña composite, suggesting that comparable cooling persists during the third La Niña peak despite the weaker La Niña forcing. Together, the MMLE simulations capture the main observed features while yielding a cleaner signal, and they suggest a lower bound on La Niña–induced GMST reductions.

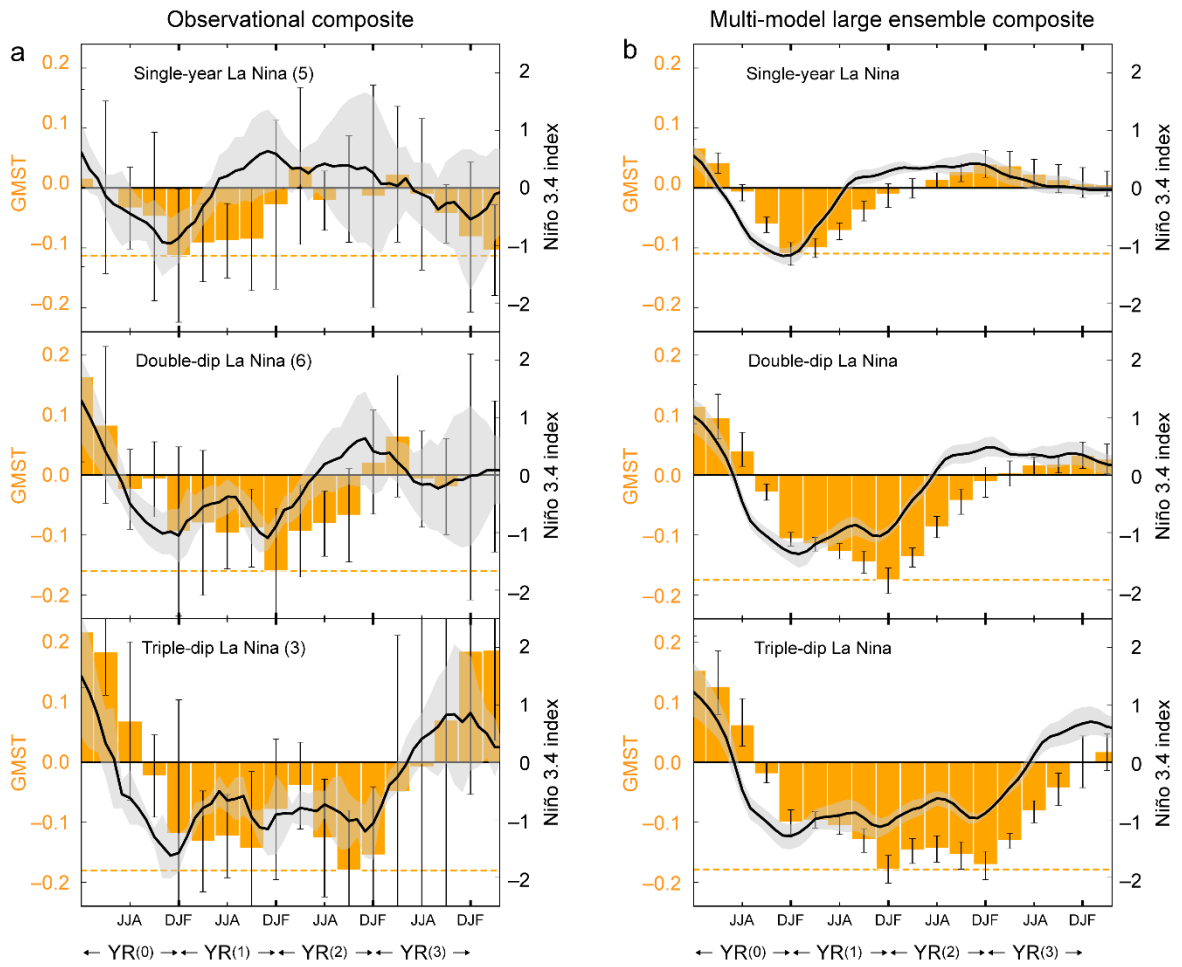

Figure 2. Evolutions of the La Niña persistency and their corresponding global-mean surface temperature (GMST) responses. (**a**) Composited evolutions of (top) single-year, (middle) double-dip, and (bottom) triple-dip La Niña events based on the observation. Orange bars and black lines represent the 3-month seasonal-mean GMST and the Niño 3.4 index (Unit: ℃), respectively. Horizontal dashed line is the GMST minimum recorded in La Niña cycle. Shadings and error bars are the 95% confidence intervals. Values in parentheses are the numbers of extracted events. (**b**) As in (a), but for multi-model large ensemble.

Focusing on the strong minimum around the second peak of multi-year La Niña, we compare the spatial patterns (Fig. 3a). In observations, the first-peak composite features pronounced cooling in the tropical Pacific and the Indian Ocean and the second-peak pattern is broadly similar but exhibits further cooling over the Atlantic. To diagnose regional roles, we decomposed GMST anomalies into basin contributions as follows:

$$T_{A_i} = \frac{1}{A_G} \int_{A_i} T \, dA, \tag{1}$$

where T is surface temperature. A is the area and the subscript i denotes each specific domain. Domains we used are the tropical Pacific (140°E-80°W, 30°S-30°N; shown as the black box in Fig. 3a), the tropical Indo-Atlantic (80°W-140°E, 30°S-30°N), and the extratropics (north of 30°N and south of 30°S). Both land and ocean regions are considered; their respective contributions are discussed later. The surface integral of T over each region is normalized by the Earth's surface area (A_G), representing its regional contribution to GMST. The sum of the tropical Pacific and the Indo-Atlantic contributions represent the tropical contribution, and the sum of all values from the three domains is equal to GMST ($= \sum_i T_{A_i}$).

This analysis indicates that tropical Pacific cooling is of comparable magnitude in the first- and second year, whereas mean cooling over the tropical Indian-Atlantic sector is greater in the second year, accounting for the additional GMST decline; extratropical contributions are smaller but of the same tendency (Fig. 3b). We note, however, that uncertainties for the regional attribution are larger than for GMST itself, and thus analysis is extended to MMLE simulations for the attribution. MMLE simulations reproduce basic features: Pacific cooling is similar across the two years, while enhanced Indian and Atlantic cooling in the second-year substantially augments the global mean response. The second-year amplification therefore reflects a pan-tropical cooling, with a key contribution from delayed ENSO-related adjustments in the Indian and Atlantic sectors outside the Pacific (Klein et al. 1999; Alexander 2002; Chowdary and Gnanaseelan 2007). From a dynamical perspective, the tropical troposphere rapidly communicates ENSO-related temperature anomalies under the weak temperature gradient (WTG) approximation (Sobel et al. 2001; Sobel 2002), in which gravity-wave adjustment, often mediated by equatorial Kelvin waves, acts to reduce zonal temperature gradients, but timescales appear to be determined by slower mixed-layer response. This timescale may be on the order of several months to about half a year in the Indian Ocean, whereas the Atlantic basin may respond on a timescale of about one year. Despite sizable observational uncertainties, both the observations and MMLE results converge on the conclusion that the GMST decrease during multi-year La Niña is explained primarily by enhanced tropical (especially Indian and Atlantic) cooling around the second year.

To consider the rapid adjustment of the tropical troposphere, the land response cannot be neglected. Here, the land and ocean contributions are quantified as the respective fractions of land and ocean cooling relative to the total pan-tropical cooling around the second year, compared to the first peak. In the tropics, about 65% of the second-peak cooling occurs over the ocean, with the remaining 35% over land in MMLE simulations. Observation suggests an

opposite partition (about 35% over the ocean and 65% over land), albeit with substantial uncertainty. In both cases, it indicates a non-negligible land contribution alongside the ocean.

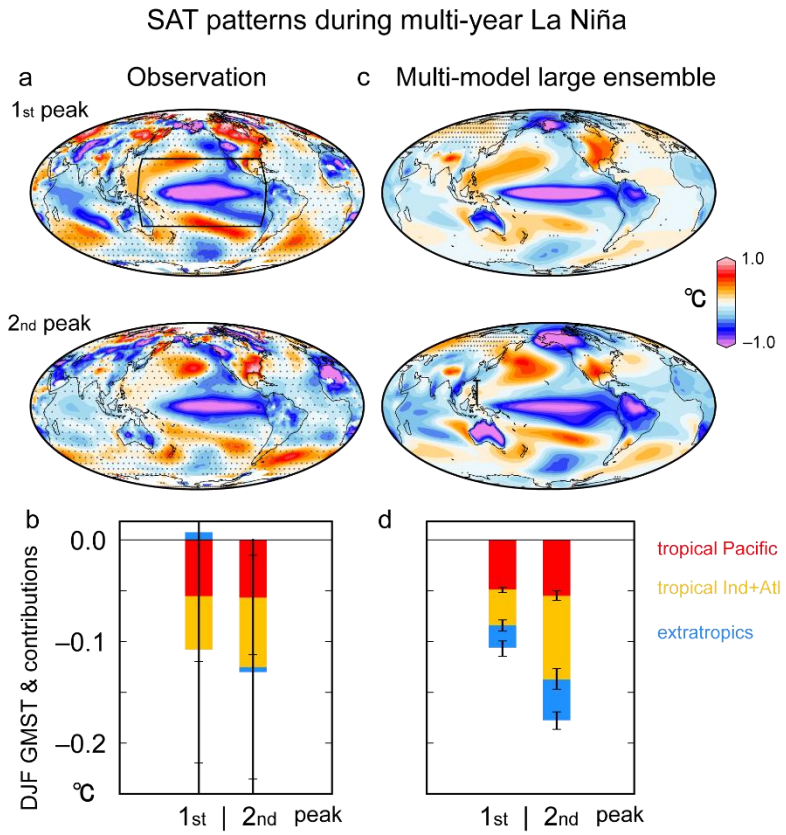

Figure 3. Multi-year La Niña-induced surface temperature cooling and its regional contribution. (**a**) Composite spatial patterns of the SAT response to a multi-year La Niña in December-January-February (DJF), derived from observation (upper: first-year peak; lower: second-year peak). Dots indicate non-significance at the 95 % confidence level. (**b**) Decrease in GMST during multi-year La Niña peaks and their domain-wise contributions. Each bar represents the composites of GMST during the La Niña peak season. Red, yellow, and blue represent contributions of three domains to GMST: the tropical Pacific (enclosed by black outline in a), the tropical Indo-Atlantic sector, and the extratropics, respectively. Error bars are the 95 % confidence intervals. (**c,d**) As in (a,b), but for multi-model large ensemble.

4. Temperature response to multi-year La Niña demonstrated by RC framework

Considering that multi-year La Niña cools pan-tropics, we demonstrate the anomalous tropical-mean surface temperature (TMST) cooling using an idealized framework. TMST is defined as the area-weighted mean over 30°S-30°N, encompassing half of Earth's surface area. We apply a Resistor-Capacitor (RC) circuit, as follows:

$$RC\frac{dV_{out}(t)}{dt} + V_{out}(t) = V_{in}(t), \quad (2)$$

where R is the resistor and C is the capacitor of the system. V_{in} and V_{out} represent the input and output voltages, respectively. As an application to the climate system, R can translate into the sensitivity of the system and C is the heat capacity. Then, RC has units of time and determines the time constant of the target. These parameters should be changed depending on the system we apply. Since this study focuses on the ENSO-forced GMST response, which is transient climate response mainly dominated in the tropics, C is the ocean mixed-layer heat capacity, calculated as $\rho c_p h$, and R is the transient climate sensitivity of tropical ocean on the seasonal to interannual time scale.

Accordingly, the RC low-pass filter framework, with the lag set by target system's heat capacity and sensitivity, can be rewritten as follows:

$$\gamma\rho c_p h\frac{d\phi_{out}}{dt} + \phi_{out} = \phi_{in}, \quad (3)$$

where, ρ is the seawater density, 1024 kg m^{-3}, c_p is the specific heat capacity at constant pressure, 4125 J kg^{-1} $°C^{-1}$. Given that we focus on the tropical response to ENSO on the year-to-year timescales, h is the tropical-mean mixed-layer depth and the γ is the sensitivity of the tropical mixed-layer to radiative forcing (°C W^{-1} m^2). Thus, $\gamma\rho c_p h$ has units of time and sets the system's *e*-folding response timescale and the equilibrium amplitude is determined by forcing amplitude. Because the eastern Pacific (180°-90°W, 15°S-15°N) for ENSO forcing occupies roughly one quarter of the tropics, local forcing is redistributed to pan-tropics, and thus we weigh the output by this fractional area (≈1/4). As illustrated by the RC-circuit analogy in Fig. 4a, ϕ_{in} is the ENSO forcing, represented here by the Niño 3.4 index, and ϕ_{out} is the TMST response.

To estimate the appropriate transient sensitivity γ, we perform 10-member ensemble abrupt CO_2 increase experiment in state-of-the-art climate model, MIROC-ES2L (Hajima et al. 2020). A CO_2 doubling experiment corresponds to an effective radiative forcing of ~3.7 W m^{-2} (Myhre et al. 1998; Gregory and Webb 2008). Each abrupt CO_2 increase experiment lasts for 5 years, focusing on seasonal to interannual responses, and is initialized from an initial condition randomly taken from a 700-year-long pre-industrial control run. γ is evaluated by the transient response of tropical ocean mixed-layer temperature to radiative forcing. Although the multi-

year La Niña-induced cooling has a land contribution (Section 3), the land surface responds more rapidly than the ocean mixed layer. Accordingly, in coupled GCM, the mixed-layer ocean response used here also reflects the influence of the land fast response. The climate response depends on the forcing type and magnitude. However, differences in efficacy across greenhouse gases and aerosol types are mostly within ~20% and are sufficiently small to neglect in this study (Hansen et al. 2005). For simplicity and clarity, we therefore adopt the abrupt CO_2 doubling experiment to estimate γ, as it is widely used in the IPCC assessments. Since there are likely other possible methods to estimate response sensitivity, it is necessary to define it for each target system and examine the sensitivity of the results. On the month-to-year timescales relevant to ENSO, the tropical mixed-layer temperature response is approximately 0.2–0.5℃ (Fig. 4b). In this study, the parameter value is not uniquely constrained and allows some extent of tolerance, given uncertainty in models and observations. Note, while the framework could be used to diagnose GMST directly, with some adjustment and tuning, we formulate it to diagnose TMST, leveraging the WTG approximation under which ENSO-related temperature response is rapidly communicated across the tropics.

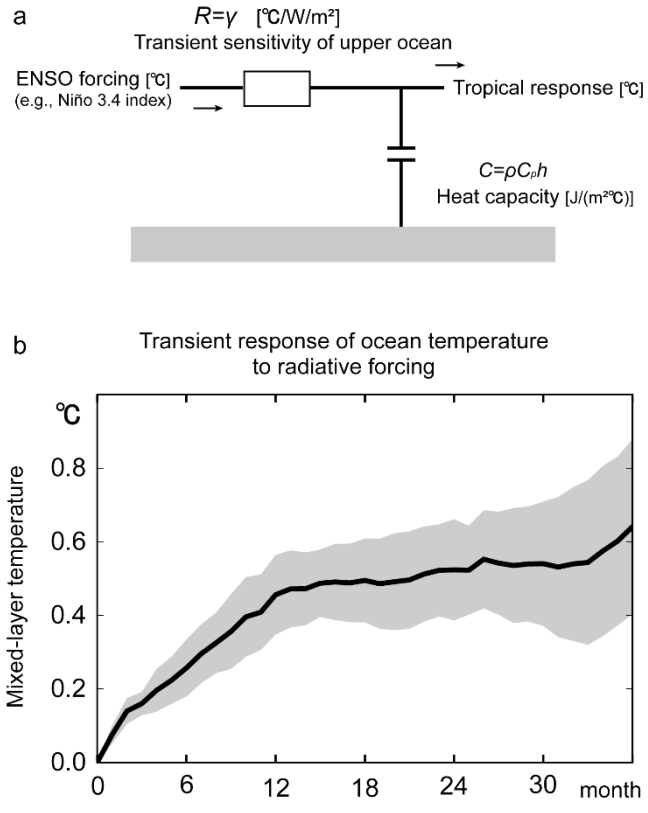

Figure 4. (**a**) Concept for application of a Resistor-Capacitor (RC) circuit to the transient ENSO impact. (**b**) Tropical-mean (30°S-30°N) mixed-layer temperature response to abrupt doubling CO_2 experiment in MIROC-ES2L, representing transient sensitivity of the system on the seasonal-to-interannual time scale. Shading shows 95% CI based on 10 ensemble simulations.

Figure 5a illustrates the RC low-pass filter's response to an idealized square wave-like ENSO forcing, with γ=0.5°C/3.7Wm^{-2} and mixed-layer depth h=30m. We assess how persistence controls TMST decreases and increases. For an idealized one-year phase transition of ENSO, the TMST lags the forcing and alternates between cooling and warming, but the sign flip occurs before the response can reach its asymptotic bounds. When the forcing persists for two years, TMST cools more than in first year and almost approaches its lower bound (and, in the opposite phase, its upper bound). Extending the persistence to three years produces little further change, as the response saturates, but persistent cooling is maintained even under weaker La Niña forcing. Despite its simplicity, this experiment captures the qualitative TMST evolution during multi-year La Niña.

We perturb the parameters γ and h to examine the interpretation (Fig. 6). It clearly demonstrates that a larger transient sensitivity of mixed-layer temperature leads to slower response. With larger γ, negative radiative feedback is weaker for a given temperature anomaly, causing the energy imbalance to persist longer and the temperature to adjust slowly. Similarly, a deeper mixed layer leads to a slower response timescale since it increases the system's heat capacity. Consequently, the response time scale becomes longer in proportion to the product of γ and h.

As a more realistic test, we force the RC low-pass filter with the La Niña composites (Fig. 5b). With appropriately chosen parameters, the RC output closely reproduces the observed TMST amplitude and phase, including the enhanced second-year cooling and the apparent lower bound. Thus, under the RC-circuit analogy, the lagged response and its saturation during multi-year La Niña are constrained by the mixed-layer heat capacity and its adjustment time at interannual scales, providing a parsimonious explanation for the GMST decline, the amplified second-year minimum, and the persistence of cooling beyond the second year even under weaker La Niña.

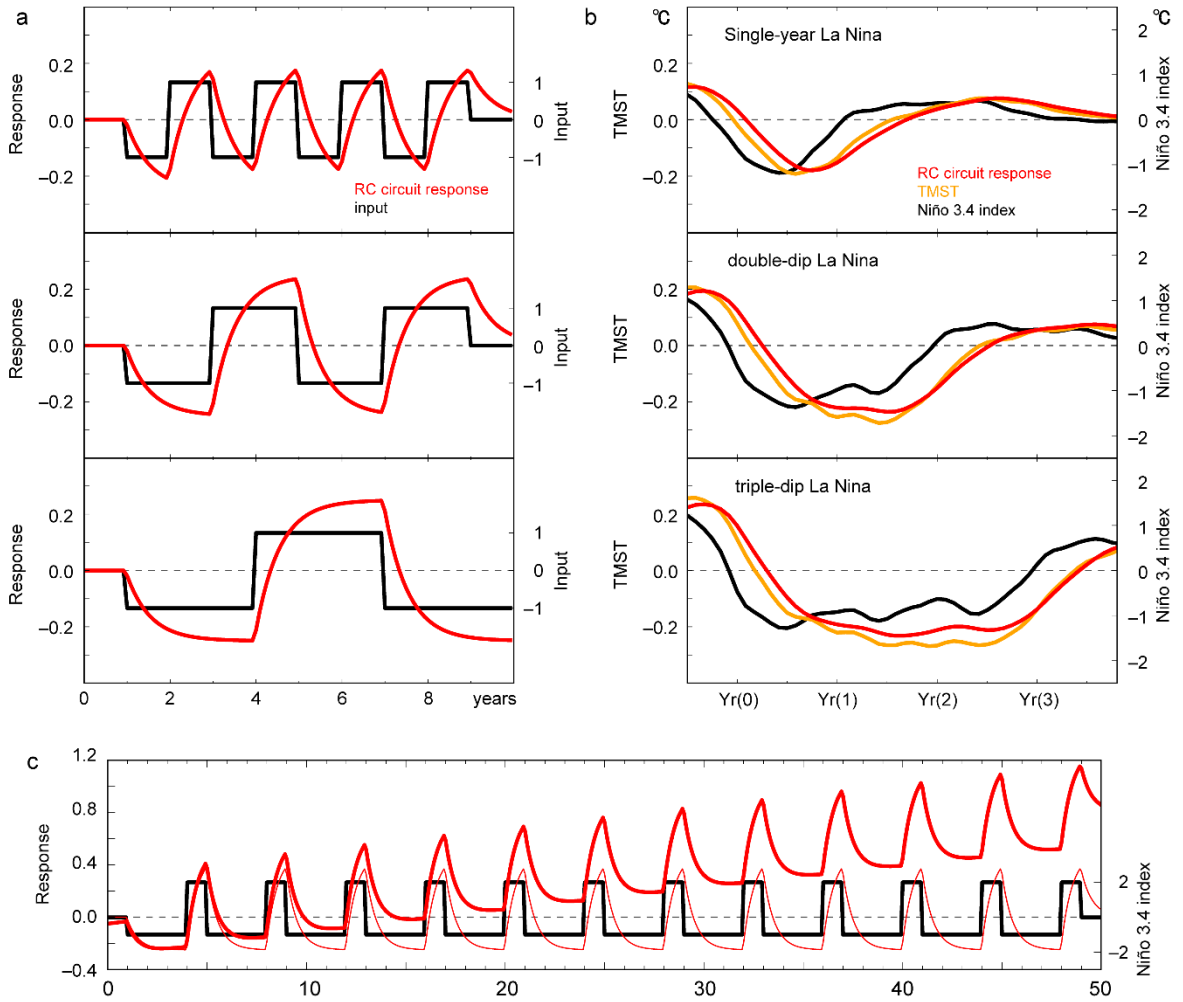

329

330 **Figure 5.** Responses of RC circuit to an idealized and realistic ENSO forcings. (**a**) Idealized square forcings
331 (black) mimic single-year La Niña (upper), double-dip La Niña (middle), triple-dip La Niña (lower panel).
332 Red lines represent the response of RC circuit. (**b**) As in (a), but for realistic Niño 3.4 forcing, derived from
333 multi-model large ensemble composite. Orange lines represent the anomalous tropical-mean surface
334 temperature (TMST) as the reference (true) value from multi-model large ensemble. (**c**) RC circuit response
335 of idealized triple-dip La Niña and strong El Niño. Thick and thin red lines are the responses with and without
336 the addition of the observed quadratic trend over the last 50 years, respectively.

337

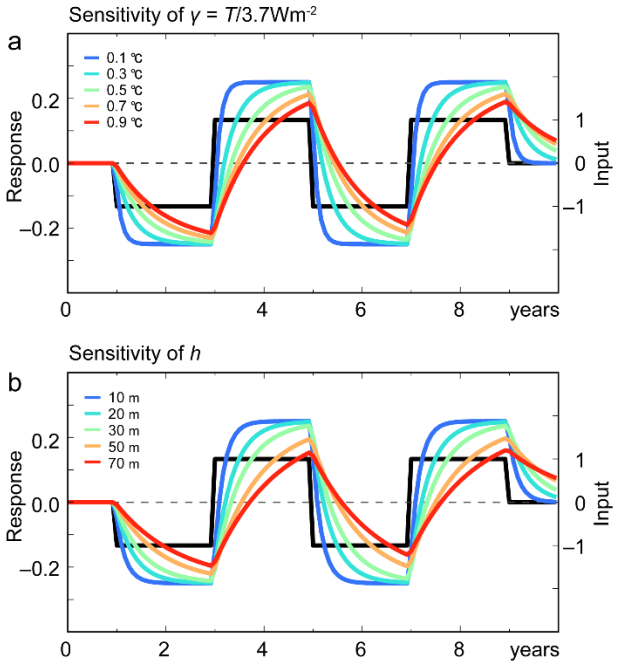

Figure 6. Parameter sensitivity of an idealized double-dip La Niña forcing in the RC circuit as a function of (**a**) perturbed γ with fixed $h = 30\text{m}$ and (**b**) perturbed h with fixed $\gamma = 0.5°\text{C}/3.7\text{Wm}^{-2}$.

5. Historical temperature response to ENSO demonstrated by RC framework

Figure 7 shows 75-year time series of ENSO, GMST, and TMST. Lead–lag correlations indicate that most GMST variability is explained by TMST and is essentially contemporaneous, consistent with the tropics covering roughly half of Earth's surface. TMST, in turn, is largely driven by ENSO and peaks a few months after the ENSO index (Klein et al. 1999; Chiang and Sobel 2002). Thus, ENSO influences GMST primarily by modulating TMST, and despite its geographic confinement to the tropical Pacific, it imprints a global signal on interannual timescales. By contrast, extratropical temperatures are largely uncorrelated with ENSO and are determined by other factors (Fig. 7c; Hurrell 1995; Thompson and Wallace 2000; Knight et al. 2006). These relationships between ENSO and regional temperature hold in MMLE simulations (Fig. S5).

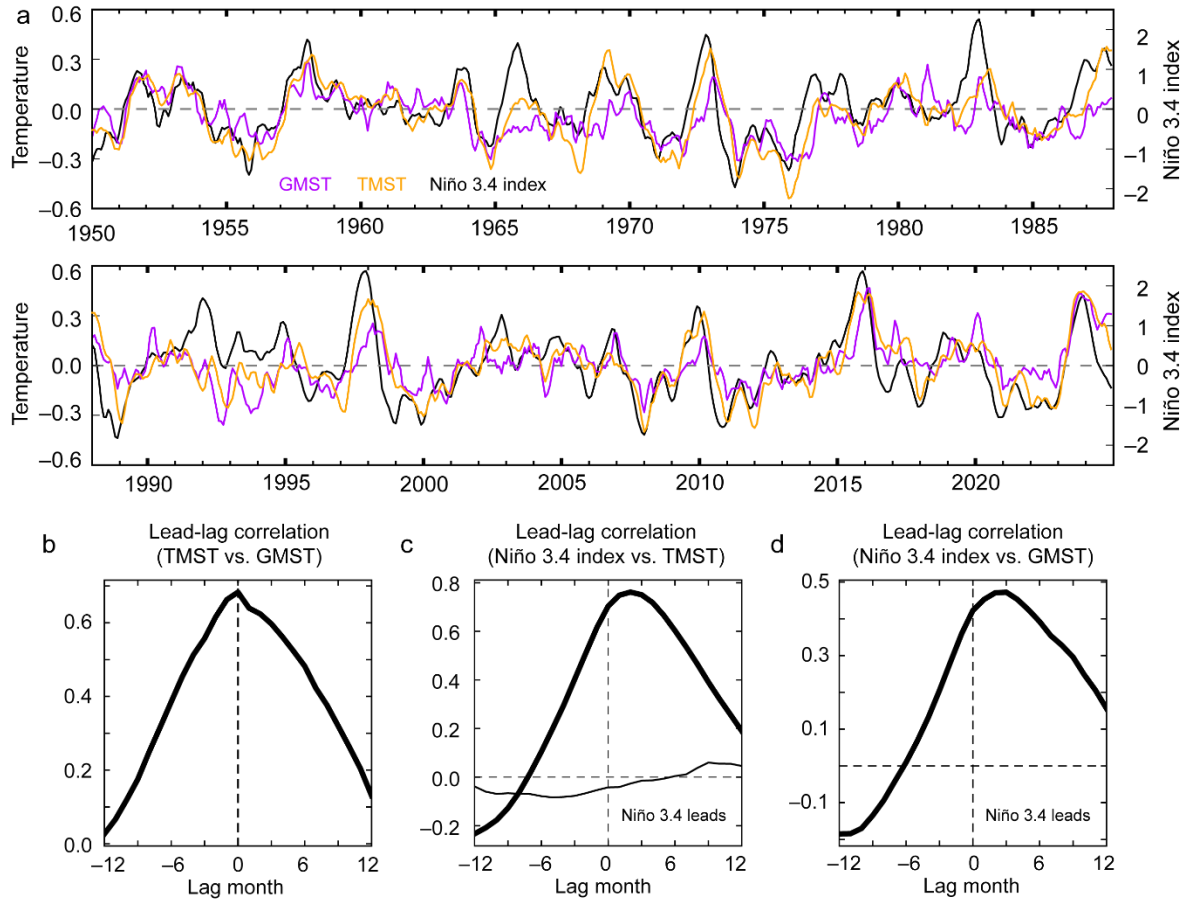

Figure 7. Relationships among observed Niño 3.4 index, GMST, and TMST (unit: °C). (**a**) 3-month running mean time series of Niño 3.4 index (black), GMST (purple), and TMST anomalies (orange). (**b**) Lead-lag correlation between TMST and GMST. (**c**) As in (b), but for Niño 3.4 index and TMST (extratropical-mean temperature; thin line). (**d**) As in (b), but for Niño 3.4 index and GMST.

Here we generalize beyond La Niña type and demonstrate the broader applicability of the RC-circuit framework to the full ENSO record. The bottom time series of Fig. 8 shows the TMST and RC response to ENSO forcing. With parameters γ =0.2°C/3.7Wm^{-2}, the RC model reproduces the TMST variability with high skill (R=0.8), while underestimating the amplitude by 18%. Therefore, RC-circuit framework can be widely applicable to global historical response to ENSO.

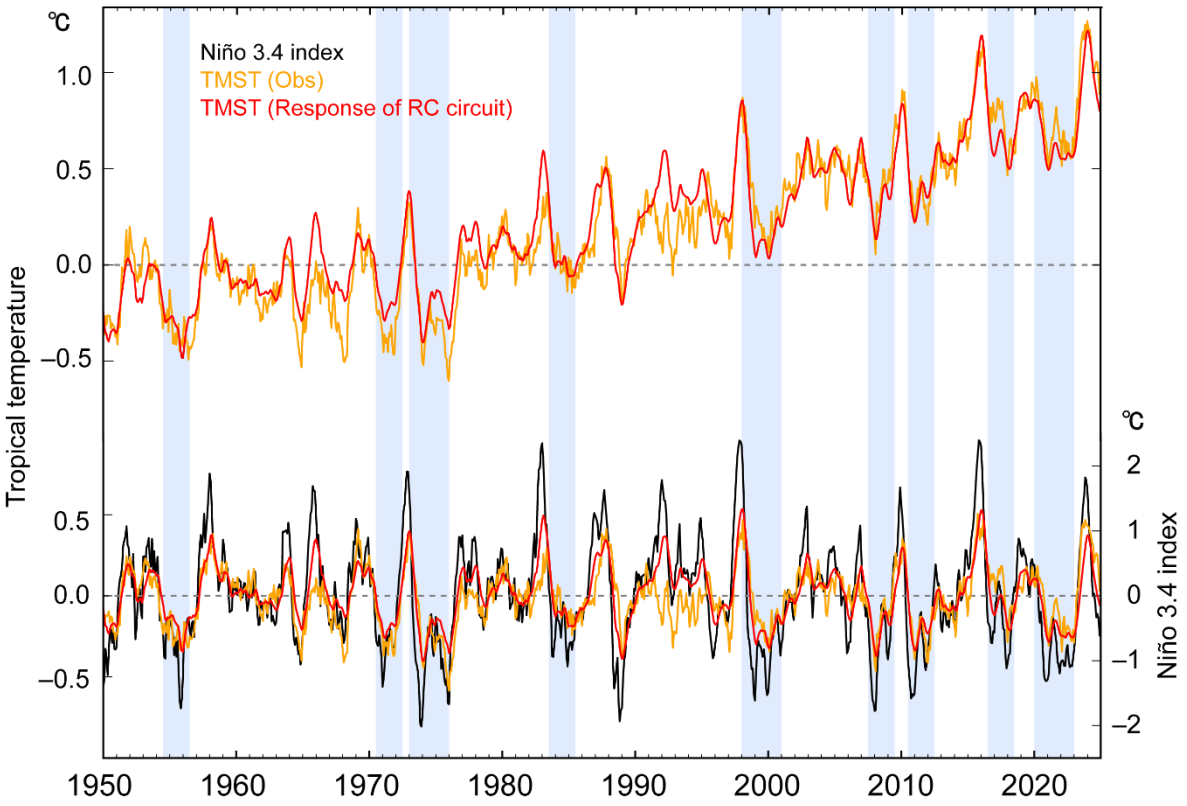

Figure 8. ENSO-forced tropical mean temperature. Lower time series show Niño 3.4 (black), observed anomalous TMST (orange), and response of RC circuit (red). Upper time series are with the addition of observed quadratic trend. Blue shadings are multi-year La Niña years.

To quantify parametric uncertainty, we perturb h from 20–60m and γ from 0.1–0.8℃ per 3.7Wm^{-2}, which are potentially within the range of observational or model uncertainty, and assess changes in correlation, amplitude, and lag (Fig. 9). Correlation remains high across this range, indicating that the RC filter robustly captures TMST variation. As expected, deeper mixed layers and larger sensitivities (which increase the effective time constant) yield a more lagged and more strongly damped response. Given typical tropical mixed-layer depths of 30–50m and the observed few-month delay of TMST relative to ENSO, a characteristic response magnitude of 0.2–0.5℃ is one reasonable parameter (Fig. 4b). However, ENSO also modulates mixed-layer depth and sensitivities vary across models, and thus parameter may be varied. Our aim is not to fine-tune unique parameters; Nonetheless, the ability of the RC-circuit framework to reproduce realistic lagged behavior and near-observed amplitudes over wide parameter ranges supports its utility as a parsimonious surrogate for ENSO-driven temperature variability. Accordingly, the RC-circuit analogy supports the view that the tropical temperature response

387 to ENSO is regulated by the climate system's interannual sensitivity and by the mixed-layer
388 response on that timescale.

389

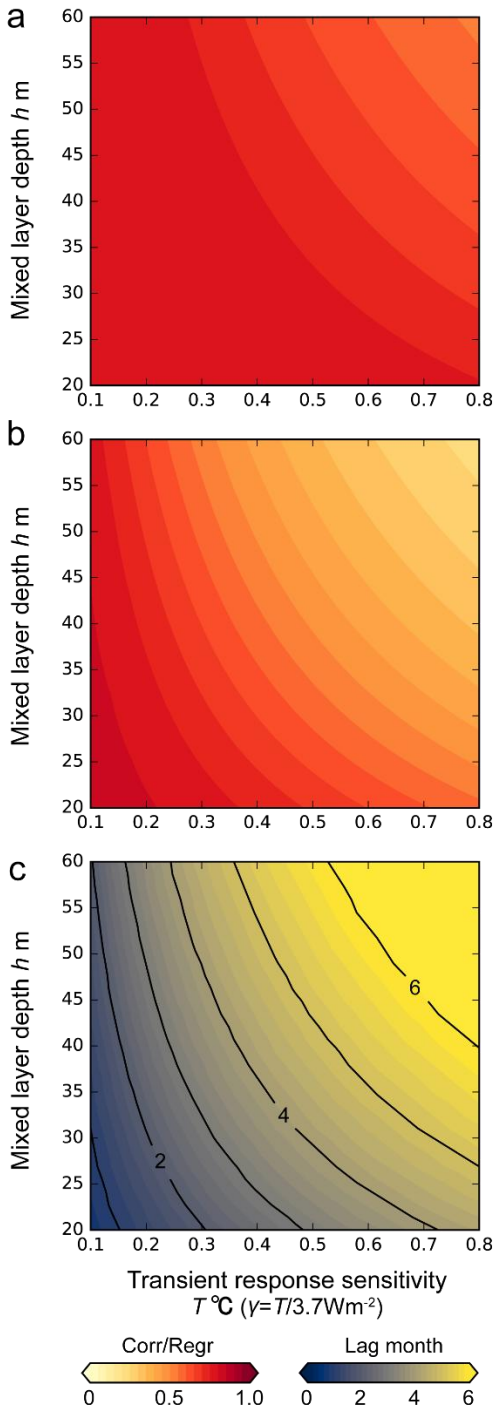

390

391 **Figure 9.** Sensitivity of the RC circuit to the two parameters. (**a**) Phase space diagram showing the
392 correlation between the observed TMST and the RC circuit response to the observed Niño 3.4 index. The x-
393 axis is sensitivity of transient response γ, and the y-axis is mixed-layer depth h. (**b,c**) As in (a), but for
394 regression coefficient (amplitude) and maximum lag month (lag in the response).

395

6. Discussion

We assess the global imprint of the recently spotlighted multi-year La Niña. While La Niña is expected to decrease GMST, differences in event persistence intensify this effect by spreading the cooling across all tropical basins; longer-lived episodes drive pan-tropical surface cooling that further decreases GMST despite weaker La Niña amplitude in the second year. This mechanism matters especially because ENSO is asymmetric—multi-year La Niña events occur more frequently than their El Niño counterparts—thereby magnifying their contribution to interannual GMST variability.

Under anthropogenic warming, multi-year La Niña episodes act to temporarily slowdown GMST. Figure 5c illustrates this phenomenon with an idealized sequence: a sustained La Niña followed by a strong El Niño. The thick curve overlays a quadratic fit to the observed GMST trend onto the RC low-pass filter's response. In this simple experiment, persistence of La Niña induces a transient slowing down in the warming trajectory, whereas the subsequent strong El Niño produces a short-lived overshoot in GMST. This evolution resembles the record-breaking, abrupt global warmth in 2023 that is followed by triple-dip La Niña (Xie et al. 2025; Esper et al. 2024; Tsuchida et al. 2026). Consistent with this analogy, adding the observed quadratic trend to the RC response, as shown in Fig. 8 upper, reproduces the sharp 2023 rise in TMST, underscoring the broader utility of the RC framework for interpreting how interannual ENSO variability interacts with the long-term warming trend. Moreover, because a multi-year La Niña often follows a strong El Niño (DiNezio and Deser 2014; Wu et al. 2019; Iwakiri and Watanabe 2021), this warming spike is transient and is mitigated by the subsequent cooling associated with the multi-year La Niña. The RC framework is commonly used in electronics, but this study highlights its usefulness in explaining GMST responses to ENSO. It can be interpreted as the zero-dimensional energy balance model (Yulaeva and Wallace 1994), but the response sensitivity and capacity of the system used as parameters are valuable for intuitive understanding and educational purposes, aiding interpretation. It also has the potential to address a broad range of problems in climate science.

Multi-year El Niños are observed, albeit less frequently. Unlike La Niña, multi-year El Niño events tend to have a larger amplitude in the second year (Wu et al. 2019; Kim and Yu 2020), and therefore an intensified second-year maximum can be readily inferred. This study does not treat multi-year El Niño, but it can be understood as a mirror image of multi-year La Niña since the GMST response to ENSO is mostly linear. Because the occurrence ratio of the observed multi-year La Niñas has been approximately twice as much as that of the multi-year El Niños,

the frequency of the episodic slowdown and the rising staircase of GMST are also expected to be asymmetric (see also Fig. 5c), unlike the expectation from the IPO-based explanation (Kosaka and Xie 2016). The frequency of strong El Niño and multi-year La Niña events is projected to increase under a high-emission scenario, potentially enhancing ENSO asymmetry (Cai et al. 2018, 2022; Geng et al. 2023). If the real world follows this scenario, episodic slowdowns of GMST and subsequent temperature increases could be observed more frequently, causing large and irregular interannual temperature variations in a changing climate.

Acknowledgments.

We appreciate the three anonymous reviewers for their constructive comments. T.I. is supported by a Grant-in-Aid from JSPS Fellows JP23KJ2168, JSPS Oversea Research Fellowships JP202560182, and the MEXT program for the advanced studies of climate change projection (SENTAN) Grant Number JPMXD0722680395. T.K is supported by JSPS KAKENHI (Grant Numbers JP23H01241 and JP23K13169), the SENTAN program, and by the Sumitomo Foundation as one of their Environmental Research Projects. We acknowledge the World Climate Research Program, which, through its Working Group on Coupled Modelling, coordinated and promoted CMIP6. We thank the climate modeling groups for producing and making available their model output, the Earth System Grid Federation (ESGF) for archiving the data and providing access, and the multiple funding agencies that support CMIP6 and ESGF. This is IPRC publication and SOEST contribution.

Data Availability Statement.

Multi-model large ensemble archive version 2 is available at https://www.cesm.ucar.edu/community-projects/mmlea/v2. Last Millennium Ensemble project is available at https://www.cesm.ucar.edu/community-projects/lme.

GISTEMPv4 and ERSSTv6 are available at https://data.giss.nasa.gov/gistemp/updates_v4 and https://www.ncei.noaa.gov/products/extended-reconstructed-sst, respectively.

Original figures are generated using Python with the matplotlib and cartopy libraries (https://matplotlib.org/, https://scitools.org.uk/cartopy).

REFERENCES

460 Alexander, M. A., 2002: The atmospheric bridge: The influence of ENSO teleconnections on
461 air–sea interaction over the global oceans. *Journal of Climate*, **15**, 27.

462 An, S.-I., and F.-F. Jin, 2004: Nonlinearity and asymmetry of ENSO. *Journal of Climate*, **17**,
463 2399–2412.

464 Bethke, I., and Coauthors, 2021: NorCPM1 and its contribution to CMIP6 DCPP. *Geosci.*
465 *Model Dev.*, **14**, 7073–7116, https://doi.org/10.5194/gmd-14-7073-2021.

466 Bjerknes, J., 1966: A possible response of the atmospheric Hadley circulation to equatorial
467 anomalies of ocean temperature. *Tellus*, **18**, 820–829, https://doi.org/10.1111/j.2153-
468 3490.1966.tb00303.x.

469 Cai, W., and Coauthors, 2018: Increased variability of eastern Pacific El Niño under
470 greenhouse warming. *Nature*, **564**, 201–206, https://doi.org/10.1038/s41586-018-
471 0776-9.

472 ——, B. Ng, G. Wang, A. Santoso, L. Wu, and K. Yang, 2022: Increased ENSO sea surface
473 temperature variability under four IPCC emission scenarios. *Nat. Clim. Chang.*,
474 https://doi.org/10.1038/s41558-022-01282-z.

475 Chiang, J. C. H., and A. H. Sobel, 2002: Tropical tropospheric temperature variations caused
476 by ENSO and their influence on the remote tropical climate. *Journal of Climate*, **15**,
477 16.

478 Chowdary, J. S., and C. Gnanaseelan, 2007: Basin-wide warming of the Indian Ocean during
479 El Niño and Indian Ocean dipole years. *Intl Journal of Climatology*, **27**, 1421–1438,
480 https://doi.org/10.1002/joc.1482.

481 Cole, J. E., 2002: Multiyear La Niña events and persistent drought in the contiguous United
482 States. *Geophys. Res. Lett.*, **29**, 1647, https://doi.org/10.1029/2001GL013561.

483 DiNezio, P. N., and C. Deser, 2014: Nonlinear controls on the persistence of La Niña.
484 *Journal of Climate*, **27**, 7335–7355, https://doi.org/10.1175/JCLI-D-14-00033.1.

485 Dommenget, D., T. Bayr, and C. Frauen, 2013: Analysis of the non-linearity in the pattern
486 and time evolution of El Niño southern oscillation. *Clim Dyn*, **40**, 2825–2847,
487 https://doi.org/10.1007/s00382-012-1475-0.

488 Esper, J., M. Torbenson, and U. Büntgen, 2024: 2023 summer warmth unparalleled over the
489 past 2,000 years. *Nature*, **631**, 94–97, https://doi.org/10.1038/s41586-024-07512-y.

490 Eyring, V., S. Bony, G. A. Meehl, C. A. Senior, B. Stevens, R. J. Stouffer, and K. E. Taylor,
491 2016: Overview of the Coupled Model Intercomparison Project Phase 6 (CMIP6)
492 experimental design and organization. *Geosci. Model Dev.*, **9**, 1937–1958,
493 https://doi.org/10.5194/gmd-9-1937-2016.

494 Fasullo, J. T., N. Rosenbloom, and R. Buchholz, 2023: A multiyear tropical Pacific cooling
495 response to recent Australian wildfires in CESM2. *Science Advances*.

Geng, T., F. Jia, W. Cai, L. Wu, B. Gan, Z. Jing, S. Li, and M. J. McPhaden, 2023: Increased occurrences of consecutive La Niña events under global warming. *Nature*, **619**, 774–781, https://doi.org/10.1038/s41586-023-06236-9.

Gregory, J., and M. Webb, 2008: Tropospheric adjustment induces a cloud component in CO2 forcing. *Journal of Climate*, **21**, 58–71, https://doi.org/10.1175/2007JCLI1834.1.

Hajima, T., and Coauthors, 2020: Development of the MIROC-ES2L Earth system model and the evaluation of biogeochemical processes and feedbacks. *Geosci. Model Dev.*, **13**, 2197–2244, https://doi.org/10.5194/gmd-13-2197-2020.

Hansen, J., and Coauthors, 2005: Efficacy of climate forcings. *J. Geophys. Res.*, **110**, 2005JD005776, https://doi.org/10.1029/2005JD005776.

Horel, J. D., and J. M. Wallace, 1981: Planetary-scale atmospheric phenomena associated with the Southern Oscillation. *Monthly Weather Review*, **109**, 813–829.

Hu, S., and A. V. Fedorov, 2017: The extreme El Niño of 2015–2016 and the end of global warming hiatus. *Geophysical Research Letters*, **44**, 3816–3824, https://doi.org/10.1002/2017GL072908.

Huang, B., and Coauthors, 2025a: Extended Reconstructed Sea Surface Temperature, Version 6 (ERSSTv6). Part I: An Artificial Neural Network Approach. *Journal of Climate*, **38**, 1105–1121, https://doi.org/10.1175/JCLI-D-23-0707.1.

——, and Coauthors, 2025b: Extended Reconstructed Sea Surface Temperature, Version 6 (ERSSTv6). Part II: Upgrades on Quality Control and Large-Scale Filter. *Journal of Climate*, **38**, 1123–1136, https://doi.org/10.1175/JCLI-D-24-0185.1.

Hurrell, J. W., 1995: Decadal Trends in the North Atlantic Oscillation: Regional Temperatures and Precipitation. *Science*, **269**, 676–679, https://doi.org/10.1126/science.269.5224.676.

IPCC, 2021: *The Physical Science Basis. Contribution of Working Group I to the Sixth Assessment Report of the Intergovernmental Panel on Climate Change*. Cambridge University Press 2391 ppp.

Iwakiri, T., and M. Watanabe, 2020: Multiyear La Niña impact on summer temperature over Japan. *Journal of the Meteorological Society of Japan*, **98**, 1245–1260, https://doi.org/10.2151/jmsj.2020-064.

——, and ——, 2021: Mechanisms linking multi-year La Niña with preceding strong El Niño. *Scientific Reports*, **11**, 11.

——, and ——, 2022: Multiyear ENSO Dynamics as Revealed in Observations, Climate Model Simulations, and the Linear Recharge Oscillator. *Journal of Climate*, **35**, 4025–4042, https://doi.org/10.1175/JCLI-D-22-0108.1.

Jeffrey, S., L. Rotstayn, M. Collier, S. Dravitzki, C. Hamalainen, C. Moeseneder, K. Wong, and J. Skytus, 2013: Australia's CMIP5 submission using the CSIRO-Mk3.6 model. *a*, **63**, 1–14, https://doi.org/10.22499/2.6301.001.

534 Jiang, N., C. Zhu, M. J. McPhaden, Z.-Z. Hu, T. Lian, C. Zhou, and D. Chen, 2025: Atypical
535 warming pattern of strong 2023-24 El Niño boosts global temperatures to new 1.5 °C
536 record. *Commun Earth Environ*, **6**, 1012, https://doi.org/10.1038/s43247-025-02971-
537 1.

538 Kay, J. E., and Coauthors, 2015: The Community Earth System Model (CESM) Large
539 Ensemble Project: A Community Resource for Studying Climate Change in the
540 Presence of Internal Climate Variability. *Bulletin of the American Meteorological*
541 *Society*, **96**, 1333–1349, https://doi.org/10.1175/BAMS-D-13-00255.1.

542 Kim, J.-W., and J.-Y. Yu, 2020: Understanding reintensified multiyear El Niño events.
543 *Geophys. Res. Lett.*, **47**, https://doi.org/10.1029/2020GL087644.

544 ——, ——, and B. Tian, 2023: Overemphasized role of preceding strong El Niño in
545 generating multi-year La Niña events. *Nat Commun*, **14**, 6790,
546 https://doi.org/10.1038/s41467-023-42373-5.

547 Kirchmeier-Young, M. C., F. W. Zwiers, and N. P. Gillett, 2017: Attribution of Extreme
548 Events in Arctic Sea Ice Extent. *J. Climate*, **30**, 553–571,
549 https://doi.org/10.1175/JCLI-D-16-0412.1.

550 Klein, S. A., B. J. Soden, and N.-C. Lau, 1999: Remote sea surface temperature variations
551 during ENSO: Evidence for a tropical atmospheric bridge. *Journal of Climate*, **12**, 16.

552 Knight, J. R., C. K. Folland, and A. A. Scaife, 2006: Climate impacts of the Atlantic
553 Multidecadal Oscillation. *Geophysical Research Letters*, **33**, 2006GL026242,
554 https://doi.org/10.1029/2006GL026242.

555 Kohyama, T., and D. L. Hartmann, 2017: Nonlinear ENSO Warming Suppression (NEWS).
556 *Journal of Climate*, **30**, 4227–4251, https://doi.org/10.1175/JCLI-D-16-0541.1.

557 Kosaka, Y., and S.-P. Xie, 2013: Recent global-warming hiatus tied to equatorial Pacific
558 surface cooling. *Nature*, **501**, 403–407, https://doi.org/10.1038/nature12534.

559 ——, and ——, 2016: The tropical Pacific as a key pacemaker of the variable rates of global
560 warming. *Nature Geosci*, **9**, 669–673, https://doi.org/10.1038/ngeo2770.

561 Larkin, N., and D. E. Harrison, 2002: ENSO warm (El Niño) and cold (La Niña) event life
562 cycles ocean surface anomaly patterns, their symmetries, asymmetries, and
563 implications. *Journal of Climate*, **15**, 1118–1140.

564 Lenssen, N. J. L., G. A. Schmidt, J. E. Hansen, M. J. Menne, A. Persin, R. Ruedy, and D.
565 Zyss, 2019: Improvements in the GISTEMP Uncertainty Model. *JGR Atmospheres*,
566 **124**, 6307–6326, https://doi.org/10.1029/2018JD029522.

567 Maher, N., and Coauthors, 2019: The Max Planck Institute Grand Ensemble: Enabling the
568 Exploration of Climate System Variability. *J Adv Model Earth Syst*, **11**, 2050–2069,
569 https://doi.org/10.1029/2019MS001639.

570 ——, and Coauthors, 2024: The updated Multi-Model Large Ensemble Archive and the
571 Climate Variability Diagnostics Package: New tools for the study of climate
572 variability and change, https://doi.org/10.5194/egusphere-2024-3684.

Meehl, G. A., J. M. Arblaster, J. T. Fasullo, A. Hu, and K. E. Trenberth, 2011: Model-based evidence of deep-ocean heat uptake during surface-temperature hiatus periods. *Nature Clim Change*, **1**, 360–364, https://doi.org/10.1038/nclimate1229.

Myhre, G., E. J. Highwood, K. P. Shine, and F. Stordal, 1998: New estimates of radiative forcing due to well mixed greenhouse gases. *Geophysical Research Letters*, **25**, 2715–2718, https://doi.org/10.1029/98GL01908.

Okumura, Y. M., P. DiNezio, and C. Deser, 2017: Evolving impacts of multiyear La Niña events on atmospheric circulation and U.S. drought. *Geophys. Res. Lett.*, **44**, https://doi.org/10.1002/2017GL075034.

Olonscheck, D., and Coauthors, 2023: The New Max Planck Institute Grand Ensemble With CMIP6 Forcing and High-Frequency Model Output. *J Adv Model Earth Syst*, **15**, e2023MS003790, https://doi.org/10.1029/2023MS003790.

Osman, M. B., J. E. Tierney, J. Zhu, R. Tardif, G. J. Hakim, J. King, and C. J. Poulsen, 2021: Globally resolved surface temperatures since the Last Glacial Maximum. *Nature*, **599**, 239–244, https://doi.org/10.1038/s41586-021-03984-4.

Pan, Y. H., and A. H. Oort, 1983: Global Climate Variations Connected with Sea Surface Temperature Anomalies in the Eastern Equatorial Pacific Ocean for the 1958–73 Period. *Monthly Weather Review*, **111**, 1244–1258.

Park, J.-H., S.-I. An, J.-S. Kug, Y.-M. Yang, T. Li, and H.-S. Jo, 2020: Mid-latitude leading double-dip La Niña. *Int J Climatol*, **41**, https://doi.org/10.1002/joc.6772.

Power, S., T. Casey, C. Folland, A. Colman, and V. Mehta, 1999: Inter-decadal modulation of the impact of ENSO on Australia. *Climate Dynamics*, **15**, 319–324, https://doi.org/10.1007/s003820050284.

Raghuraman, S. P., B. Soden, A. Clement, G. Vecchi, S. Menemenlis, and W. Yang, 2024: The 2023 global warming spike was driven by the El Niño–Southern Oscillation. *Atmos. Chem. Phys.*, **24**, 11275–11283, https://doi.org/10.5194/acp-24-11275-2024.

Rodgers, K. B., J. Lin, and T. L. Frölicher, 2015: Emergence of multiple ocean ecosystem drivers in a large ensemble suite with an Earth system model. *Biogeosciences*, **12**, 3301–3320, https://doi.org/10.5194/bg-12-3301-2015.

Sobel, A. H., 2002: The ENSO signal in tropical tropospheric temperature. *Journal of Climate*, **15**, 5.

——, J. Nilsson, and L. M. Polvani, 2001: The weak temperature gradient approximation and balanced tropical moisture waves. *Journal of the Atmospheric Sciences*, **58**, 16.

Stouffer, S. A., E. A. Suchman, L. C. Devinney, S. A. Star, and R. M. Williams, 1949: The Americal Soldier: Adjustment during Army life. *Princeton Univ. Press*, **1**, 486.

Sun, L., M. Alexander, and C. Deser, 2018: Evolution of the Global Coupled Climate Response to Arctic Sea Ice Loss during 1990–2090 and Its Contribution to Climate Change. *J. Climate*, **31**, 7823–7843, https://doi.org/10.1175/JCLI-D-18-0134.1.

611 Swart, N. C., and Coauthors, 2019: The Canadian Earth System Model version 5
612 (CanESM5.0.3). *Geosci. Model Dev.*, **12**, 4823–4873, https://doi.org/10.5194/gmd-
613 12-4823-2019.

614 Tatebe, H., and Coauthors, 2019: Description and basic evaluation of simulated mean state,
615 internal variability, and climate sensitivity in MIROC6. *Geosci. Model Dev.*, **12**,
616 2727–2765, https://doi.org/10.5194/gmd-12-2727-2019.

617 Taylor, K. E., R. J. Stouffer, and G. A. Meehl, 2012: An Overview of CMIP5 and the
618 Experiment Design. *Bulletin of the American Meteorological Society*, **93**, 485–498,
619 https://doi.org/10.1175/BAMS-D-11-00094.1.

620 Thompson, D. W. J., and J. M. Wallace, 2000: Annular Modes in the Extratropical
621 Circulation. Part I: Month-to-Month Variability*. *J. Climate*, **13**, 1000–1016,
622 https://doi.org/10.1175/1520-0442(2000)013%3C1000:AMITEC%3E2.0.CO;2.

623 ——, ——, P. D. Jones, and J. J. Kennedy, 2009: Identifying Signatures of Natural Climate
624 Variability in Time Series of Global-Mean Surface Temperature: Methodology and
625 Insights. *Journal of Climate*, **22**, 6120–6141,
626 https://doi.org/10.1175/2009JCLI3089.1.

627 Timmermann, A., and Coauthors, 2018: El Niño–Southern Oscillation complexity. *Nature*,
628 **559**, 535–545, https://doi.org/10.1038/s41586-018-0252-6.

629 Trenberth, K. E., J. M. Carton, D. P. Stepaniak, and S. Worley, 2002: Evolution of El Niño-
630 Southern Oscillation and global atmospheric surface temperatures. *Journal of*
631 *Geophysical Research*, **107**, 5.

632 Tsuchida, K., Y. Kosaka, and S. Minobe, 2026: Multi-year La Niña–El Niño transition
633 influenced Earth's extreme energy uptake in 2022–2023. *Nat. Geosci.*,
634 https://doi.org/10.1038/s41561-026-01921-6.

635 Walker, G. T., 1923: Correlation in seasonal variations of weather, VIII: A preliminary study
636 of world weather. *Mem. Indian Meteor. Dept.*, **24**, 75–131.

637 Watanabe, M., H. Shiogama, H. Tatebe, M. Hayashi, M. Ishii, and M. Kimoto, 2014:
638 Contribution of natural decadal variability to global warming acceleration and hiatus.
639 *Nature Clim Change*, **4**, 893–897, https://doi.org/10.1038/nclimate2355.

640 Wu, X., 2020: Duration of El Nino and La Nina events: Mechanisms and multiyear
641 predictability. The University of Texas at Austin.

642 ——, Y. M. Okumura, and P. N. DiNezio, 2019: What controls the duration of El Niño and
643 La Niña events? *Journal of Climate*, **32**, 5941–5965, https://doi.org/10.1175/JCLI-D-
644 18-0681.1.

645 Xie, S.-P., A. Miyamoto, P. Zhang, Y. Kosaka, Y. Liang, and N. J. Lutsko, 2025: What made
646 2023 and 2024 the hottest years in a row? *npj Clim Atmos Sci*, **8**, 117,
647 https://doi.org/10.1038/s41612-025-01006-y.

Yulaeva, E., and J. M. Wallace, 1994: The signature of ENSO in global temperature and precipitation fields derived from the microwave sounding unit. *Journal of Climate*, **7**, 1719–1736.

Zhang, Y., J. M. Wallace, and D. S. Battisti, 1997: ENSO-like interdecadal variability: 1900–93. *Journal of Climate*, **10**, 1004–1020.

Ziehn, T., and Coauthors, 2020: The Australian Earth System Model: ACCESS-ESM1.5. *J. South. Hemisph. Earth Syst. Sci.*, **70**, 193–214, https://doi.org/10.1071/ES19035.